Vortex-Ring Structure-Transition in a Jet Emitting Discrete Acoustic Frequencies

A. B. C. Anderson

Citation: The Journal of the Acoustical Society of America **28**, 914 (1956); doi: 10.1121/1.1908516
View online: https://doi.org/10.1121/1.1908516
View Table of Contents: http://asa.scitation.org/toc/jas/28/5
Published by the Acoustical Society of America

simply related to the space derivative; it has been found that the speed of propagation is, in fact, an average of the speed of the ends. It is obvious that displacement is not an attribute on which to base an analysis.

A conclusion to be drawn from this investigation is that the significant relationships that exist in the sound field can be represented unambiguously in simple space-time coordinates. It may be convenient or necessary to investigate either the phenomena at a specific point in the field or the phenomena in a specific mass-element, but there is certainly no necessity to employ any but a space-time coordinate system.

THE JOURNAL OF THE ACOUSTICAL SOCIETY OF AMERICA VOLUME 28, NUMBER 5 SEPTEMBER, 1956

Vortex-Ring Structure-Transition in a Jet Emitting Discrete Acoustic Frequencies

A. B. C. ANDERSON*
Michelson Laboratory, U. S. Naval Ordnance Test Station, China Lake, California
(Received February 9, 1956)

Visualization of the vortex flow pattern in typical jets emitting jet tones was made by means of shadowgraph techniques to show the nature of the ever present process of vortex coalescence in the jet and how this determines the values of the eigenton sound frequencies radiated by the jet. These frequencies are superimposed on the noise background radiated by the jet. The dependence of (a) vortex shedding frequency from the orifice, (b) jet-tone frequencies, and (c) translational velocity of the vortices on Reynolds number (Re) is shown.

These studies were carried out with carbon dioxide jets discharging into the atmosphere. The flow channel geometry consisted of an orifice plate containing a sharp-edged, circular orifice, 0.250 in. in diameter and 0.093 in. thick attached to a large stilling tank partly filled with sound-absorbing material to eliminate any effects of cavity resonance on the jet. The studies were carried out over the range from Re zero to Re 7000, where $\mathrm{Re}=v\rho t/\mu$ and v is mean velocity of discharge of jet; ρ, gas density; t, orifice plate thickness, and μ, gas viscosity.

INTRODUCTION

As the velocity of flow of a fluid through an orifice is gradually increased the component frequencies of the jet tone radiated also increase more or less gradually.[1,2] This increase usually continues over a considerable range of Re until the amplitudes of the discrete frequencies finally merge into the turbulent noise background emitted by the jet.

If the same aerodynamic mechanism is involved in the generation of jet tones as has been shown to be involved in the generation of pipe tones, then jet tones are created aerodynamically by the periodic shedding of vortices from the orifice.[3-7] Jet tones generally are weaker, more unstable, and uncertain, and also do not occur over as great a range of Re as pipe tones which always involve the stabilizing influence of a resonant cavity.

For relatively thin orifice plates, studies have shown that the orifice number tf/u or $tf/(\Delta p/\rho)^{\frac{1}{2}}$ is relatively constant over a wide range of Re,[1] where t is the orifice plate thickness; f, one of the discrete frequency components of the jet tone; u, the jet flow velocity; Δp, the pressure difference across the orifice plate; and ρ, the density of the fluid. For relatively thick orifices a similar expression holds, except that orifice diameter and not orifice plate thickness is used as the characteristic length in the orifice number.

A jet tone usually consists of a number of discrete frequency components which are harmonics or subharmonics of a so-called fundamental frequency H_1. The amplitudes of the harmonics decrease in the order H_1, $2H_1$, $3H_1$, etc. The frequencies of the more common subharmonics are $H_1/2$, $H_1/3$, $\frac{2}{3}H_1$, $H_1/4$, etc., whose amplitudes may be even greater, and generally, are far more unsteady and fluctuating with time than H_1 and the harmonics.

It appears unnecessary to assume that a separate vortex is shed for each harmonic observed in a jet tone.[1] Several harmonic tones may arise from a single succesion of uniformly spaced vortices. The periodic shedding of vortices from the orifice gives rise to a periodic succession of acoustic impulses, of frequency H_1 radiated from the jet, which gives rise to the harmonic tones H_1, $2H_1$, $3H_1$, etc. Also, each of the vortices shed may not have exactly the same strength as adjacent ones. If, for example, alternate vortices are strong, one might expect the appearance of the subharmonic $H_1/2$. Kelvin's expression

$$v=\frac{k}{4\pi R}\left[\ln\frac{8R}{r}-\frac{1}{4}\right]$$

* At present with Aerodynamics Development Group, North Aviation Inc., International Airport, Los Angeles 45, California.

[1] A. B. C. Anderson, J. Acoust. Soc. Am. **26**, 21–25 (1954).
[2] A. B. C. Anderson, J. Acoust. Soc. Am. **27**, 13–21 (1955).
[3] Henning von Gierke, "Über schneidentöne an kreisrunden gas-strahlen und ebenen lamellen," Dissertation, Technischen Hochschule, Karlsruhe (1944).
[4] Henning von Gierke, Z. angew. Phys. **2**, 97–106 (1950).
[5] A. B. C. Anderson, J. Acoust. Soc. Am. **25**, 626–631 (1953).
[6] A. B. C. Anderson, J. Acoust. Soc. Am. **25**, 541–545 (1953).
[7] A. B. C. Anderson, J. Acoust. Soc. Am. **24**, 675–681 (1952).

was originally derived for the axial velocity of translation[8] of an isolated vortex ring in a perfect fluid. The radius r of the circular cross section (core) of the vortex is assumed small compared with the ring-radius R, and k is the strength of the whole vortex. In instances where this expression has been used for calculating the translational velocity of the vortices in a pipe-tone jet, fair agreement was found with experiment in the trend of the dependence of the vortex translational velocity v on Re.[9] Where the vortices in the jet are close together and where their interaction leads rather quickly to vortex coalescence, as in the present studies, the extent of the validity of this expression has not yet been demonstrated experimentally. Experimental studies have indicated that the ratio of vortex translational velocity of the vortices in a pipe-tone jet to jet stream velocity is fairly constant and independent of Re over the range of variables investigated.

The present paper is concerned with visualization of the vortex flow pattern in typical jet-tone jets by means of shadowgraph techniques. This allows one to observe the transition in form of the vortex pattern resulting from the ever present process of vortex coalescence in the jet. The multiplicity of vortex separations downstream in the jet resulting from vortex coalescence will be found, from the present studies, to be the cause for the appearance of the subharmonics generally radiated from jet-tone jets. The present studies also lead to a determination of the dependence of the downstream translational velocity of the vortices on Re.

APPARATUS

These studies were carried out with carbon dioxide jets discharging into the atmosphere through a very carefully made sharp-edged, circular orifice, 0.250 in. in diameter and 0.093 in. thick, attached to a large stilling tank. The tank was carefully lined to eliminate any cavity resonances that might affect the sound radiation from the jet. In other respects the equipment was the same as described elsewhere.[9] Metric measurements on the shadowgraphs were greatly facilitated by the use of a Universal Telereader-Type 17-A developed by the Telecomputer Corporation, Burbank, California. An expression of appreciation to Andrew Ballew of the Research Department for carrying out much of the experimental work is hereby acknowledged.

EXPERIMENTAL RESULTS

Figures 1 to 10 show typical side views of the jet-tone vortex ring structure observed. The jets discharge upward from the orifice located at the bottom of each shadowgraph. The shadowgraphs occur in pairs, the right hand showing the jet at a slightly later time than the left.

The time interval between each shadowgraph pair was determined as described[9] elsewhere. The principle jet-tone frequencies observed, and the corresponding Re are shown in the figure legends. The length scale, on the side of each photograph and used in evaluating the geometry and velocity of the vortices, has here been trimmed off for economy of space.

The minimum vortex separations l_0 in the jet are always found upstream in the region adjacent to the orifice which frequently extends a short distance farther downstream. These separations generally correspond to the normal vortex shedding frequency f_0, from the orifice which frequency is determined by the orifice number $tf_0/u=$ constant, approximately. Occasionally there are deviations from this minimum vortex shedding interval. Vortex shedding intervals of $\frac{2}{3}l_0$, $2l_0$, etc. are occasionally observed, especially at the higher Re. This entails shedding frequencies $\frac{3}{2}f_0$, $2f_0$, etc., respectively.

In the following where two different figures are used to illustrate successive stages in a given process of vortex coalescence, the two figures do not actually show successive stages of the same jet. They generally have been taken many minutes apart although the two shadowgraphs in any one figure were taken only a fraction of a millisecond apart. The two figures are presented together because the second happens to illustrate and carry to completion a particular process of vortex coalescence initiated in the first. This explains why sometimes only a part of the two figures seems related.

As the vortices move downstream, discrete transitions from the normal vortex shedding separation l_0 occur as a result of vortex coalescence. Figures 1 and 2, taken at widely different times showing vortex separation intervals l_0, $2l_0$, and $4l_0$, illustrate successive stages in one form of transition from l_0 to $2l_0$ and then to $4l_0$. Vortex 2 (in left shadowgraph, Fig. 1) is interacting mainly with vortex 3, to take the form in the right shadowgraph a moment later. The right-hand shadowgraph, (Fig. 2) shows annihilation of identity of vortex 2 carried to completion. The circulation of vortex 2 appears to have become associated mainly with vortex 3. Vortex 4 (Fig. 2) left shadowgraph, is also in a process of interaction that leads eventually to loss of its identity, an increase in diameter of vortex 5, and a doubling of the vortex separation interval to $4l_0$ on right.

Figures 3 and 4 illustrate a common form of vortex coalescence often observed at the lower Re. Vortices 1, 2, 3, and 4 (Fig. 3) left shadowgraph, were originally equidistant with a separation l_0. Vortices 2 and 3 are now interacting so that the radius of vortex 2 becomes smaller causing vortex 2 to speed up, and the radius of vortex 3 becomes larger, causing vortex 3 to slow up until both coalesce into vortex 2, 3 in right shadowgraph. This type of vortex coalescence involving three normal vortex intervals l_0 leads to two intervals each having the length $\frac{3}{2}l_0$. Vortices 2, 3, and 4 (Fig. 4) show

[8] Horace Lamb, *Hydrodynamics* (Dover Publications, New York, 1945), pp. 241, 242.
[9] A. B. C. Anderson, J. Acoust. Soc. Am. 27, 1048 (1955).

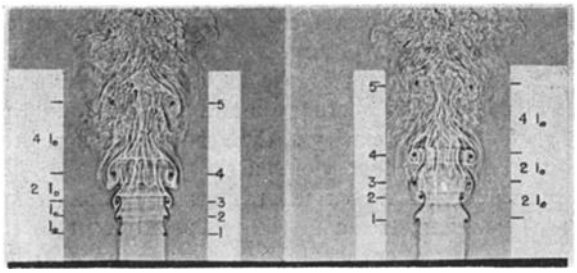

FIG. 1. $f=880^*$, 1350, 1940 cps; Re=2700; $\Delta t=0.267\times10^{-3}$ sec; (A970).

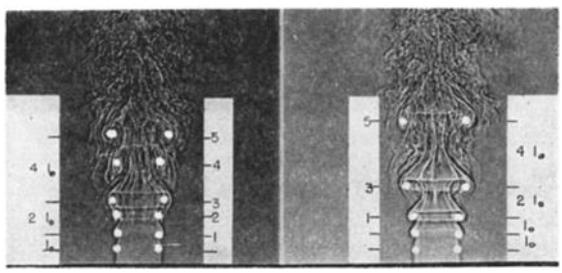

FIG. 2. $f=880^*$, 1350, 1940 cps; Re=2700; $\Delta t=0.260\times10^{-3}$ sec; (B6).

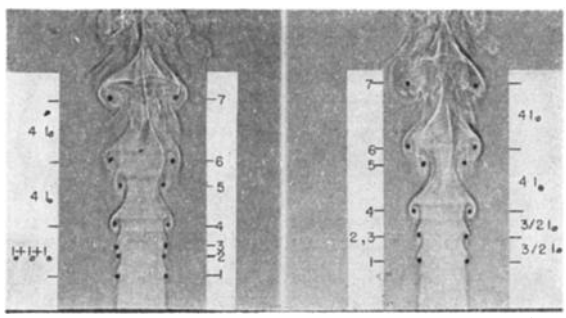

FIG. 3. $f=$none audible; Re=1160; $\Delta t=0.513\times10^{-3}$ sec; (A938).

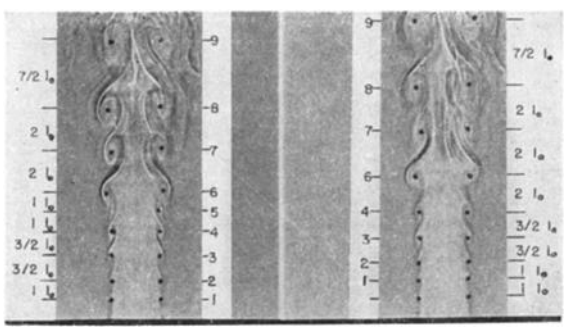

FIG. 4. $f=$none audible; Re=1200; $\Delta t=0.492\times10^{-3}$ sec; (B66).

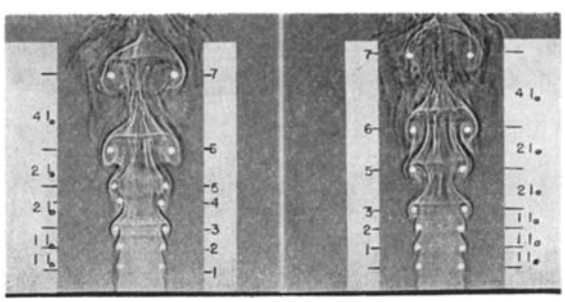

FIG. 5. $f=$none audible; Re=1500; $\Delta t=0.458\times10^{-3}$ sec; (B63).

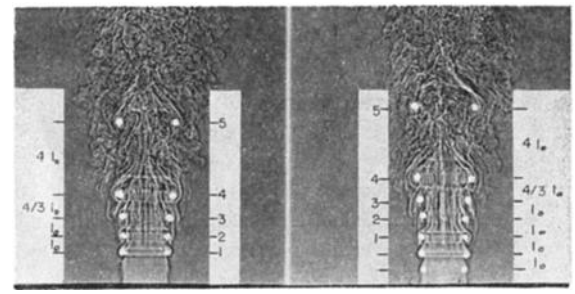

FIG. 6. $f=1337$, 1782,2140, 2673^*, 3563, 5350 cps; Re=3320; $\Delta t=0.2115\times10^{-3}$ sec; (B25).

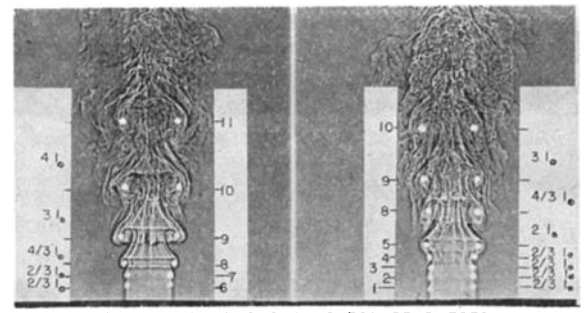

FIG. 7. $f=1337$, 1782, 2140, 2673^*, 3563, 5350 cps; Re=3320; $\Delta t=0.598\times10^{-3}$ sec; (B30).

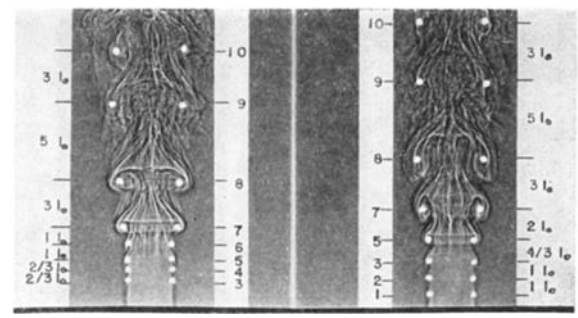

FIG. 8. $f=665^*$; Re=1920; $\Delta t=0.431\times10^{-3}$ sec; (B49).

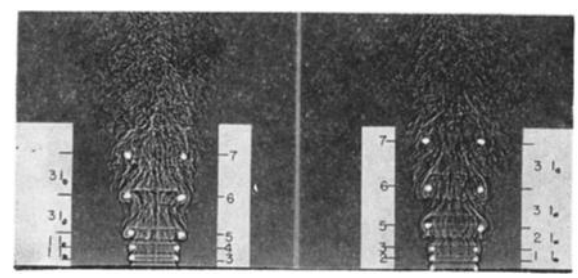

FIG. 9. $f=2175$, 2830, 3190, 4250, 5700^*, 6370 cps; Re=4610; $\Delta t=0.128\times10^{-3}$ sec; (B100).

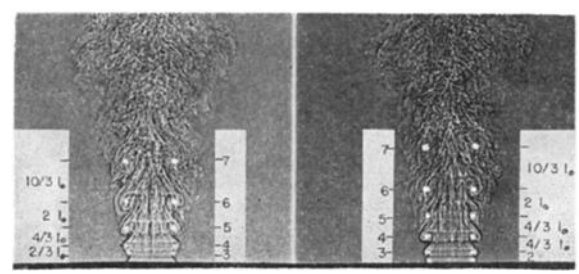

FIG. 10. $f=2175$, 2830, 3190, 4250, 5700^*, 6370 cps; Re=4610; $\Delta t=0.110\times10^{-3}$ sec; (B110).

uniform downstream movement of this newly created vortex interval.

Figure 3 also shows advanced stages of vortex coalescence. Vortex 5 originally separated $2l_0$ from vortex 4 and $2l_0$ from vortex 6 is in process of coalescing with vortex 6 eventually to create vortex interval $4l_0$ on right shadowgraph. Vortex intervals 6–7 already are $4l_0$. Figure 4 shows vortex 5 losing its identity in left shadowgraph and adding its circulation to vortex 6 to form the separation $2l_0$ between vortices 4 and 6 in right shadowgraph. The vortex intervals 6–7, and 7–8 are both $2l_0$.

Figure 5 illustrates later stages in the transition from vortex intervals l_0 to $2l_0$ to $4l_0$. Vortex 4 is slowly accelerating towards 5 adding to the circulation of vortex 5, finally to lose its identity in the right shadowgraph, leaving the vortex interval $2l_0$. Vortex interval 6–7 appears to have resulted from coalescence of two such vortex intervals as 3–5 and 5–6.

Occasionally the jet will depart from discharging vortices at the normal interval of separation l_0, and instead, discharge them at some other submultiple interval such as $\frac{2}{3}l_0$. Figures 6 and 7 are two sets of shadowgraphs of the same jet at different times in which this occurs. Vortex interval 3–4 (Fig. 6) is $4/3l_0$, the result of the coalescence of 2 intervals of length $\frac{2}{3}l_0$ each, whereas, 4–5 is the result of the coalescence of 4 normal intervals l_0. Figure 7, on the other hand, shows a number of intervals of length $\frac{2}{3}l_0$, just above the orifice. Such a sequence doubtlessly has coalesced to give the larger intervals above. For example, interval 8–9 is $2 \times \frac{2}{3}l_0 = 4/3l_0$, and intervals 5–6, 6–7, and 7–8 doubtlessly have combined to give $3 \times \frac{2}{3}l_0 = 2l_0$ which is interval 5–8 on right. Intervals 2–3, 3–4, and 4–5 on right already appear to be in initial stages of coalescence. Interval 10–11 may have combined from 2 such intervals as 5–8 or four of the normal intervals l_0.

In Fig. 8 vortex intervals 3–4 and 4–5, each having length $\frac{2}{3}l_0$ on the left, are seen to have coalesced on the right into the single interval 3–5 having the length $4/3l_0$. Above these on left are intervals 5–6 and 6–7, each having the normal length l_0, which have coalesced on the right into the single interval 5–7 having a length $2l_0$. Interval 8–9 which has a length $5l_0$ may have coalesced earlier from two shorter intervals like 5–7 and 7–8.

Figures 9 and 10 show presence of vortex coalescence at the highest Re in the series of shadowgraphs, Figs. 1 to 10. Vortex intervals 3–4 and 4–5 on the left (Fig. 9) each of length l_0, have coalesced on the right into the single interval 3–5 of length $2l_0$. The two longer intervals, 5–6 and 6–7, preserve their identity as they proceed downstream on right. At this Re the jet does not always, however, shed its vortices at the normal vortex separation l_0. Occasionally (Fig. 10) it sends out a train whose separation is $\frac{2}{3}l_0$. Thus, vortex intervals 2–3 part of which is below figure as shown and 3–4, on left, whose lengths are each $\frac{2}{3}l_0$ have coalesced on right to the single interval 3–4 having a length $4/3l_0$. Vortex separation 5–6, having a length $2l_0$, in this case probably resulted from the coalescence of three intervals having each a length $\frac{2}{3}l_0$ while vortex separation 6–7, having a length $10/3l_0$, probably coalesced from two vortex intervals similar to 4–5, of length $4/3l_0$, and 5–6, of length $2l_0$.

In general, the higher the Re the shorter the length of the well-defined vortex train in the jet.

Owing to vortex coalescence in a jet (Figs. 1 to 10), longer vortex separations are always evolved from the normal separation l_0 of the vortices just emerging from the orifice. Only a few different discrete values of vortex separation, however, and not an unlimited number are likely to occur. These discrete values are multiples of the normal separation l_0 being determined by the most likely ways the vortices in a train having the vortex separation l_0 (or possibly $\frac{2}{3}l_0$ or $\frac{1}{2}l_0$ etc.) will coalesce with each other upon emergence from the orifice. Each of these vortex intervals appears to give rise to one of the discrete audible acoustic frequencies found in the jet tone if the interval occurs frequently enough in the jet. All of these have a lower frequency than the one corresponding to the vortex separation l_0 immediately adjacent to the orifice. The vortex shedding frequencies associated with the observed vortex separations were calculated from information, contained in shadowgraph pairs such as Figs. 1 to 10, which consisted of the vortex separation and the vortex translational velocity of the vortices. Calculations were carried out on many shadowgraph pairs covering a wide range of Re. The results giving the dependence of the observed vortex shedding frequencies on Re are indicated by the points plotted in Fig. 11.

Although vortices were observed in the jets down to the lowest Re, audible jet tones were generally not heard much below Re 2000. The lines passing through the different vortex shedding frequencies observed in the audible range have a distinctly different slope than in the inaudible. The lines in the audible range (Fig. 11) are indicated by solid lines and intersect the horizontal axis at approximately Re 1150, whereas, the lines in the inaudible range indicated by dotted lines appear to intersect at the origin Re zero. The highest frequency most frequently encountered at each Re is seen to be the frequency f_0 corresponding to the normal separation

FIGS. 1–10. Shadowgraph side views of typical jet-tone vortex-ring structures observed. Jets are all discharging upward from the orifice located at bottom of each shadowgraph. The shadowgraphs occur in pairs, the right hand showing the jet at a slightly later time Δt than the left. Jet-tone sound frequencies as measured by a microphone are given below each figure. The frequency of the most intense tone observed is starred in each case. The centers of the vortex cores are emphasized by a white or black dot. The multiple nature of each of the vortex separations is expressed on sides of the shadowgraphs in terms of l_0. The same number is assigned to the same vortex on the left shadowgraph as on the right shadowgraph taken a time Δt later. The number in parenthesis denotes the laboratory notebook number of the shadowgraph picture.

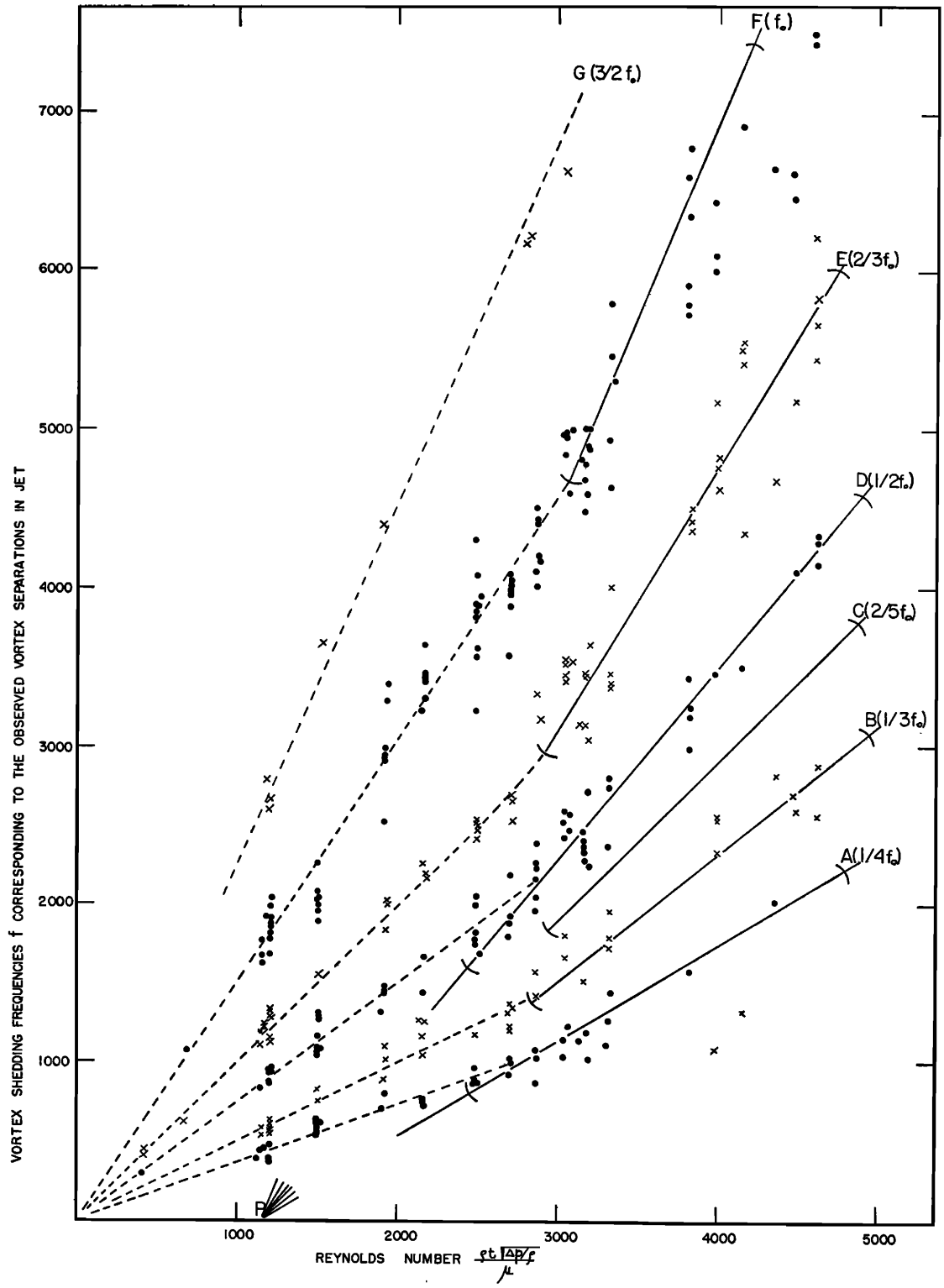

FIG. 11. Dependence of vortex shedding frequency (dots or crosses) on Reynolds number. Solid lines show dependence of the audible frequencies, radiated by jet, on Reynolds number. These solid lines pass through the mean of the points or crosses, and their prolongation downward intersects at point P around Re 1150. Dots and crosses are used to separate visually, more easily, the different groupings of vortex shedding frequency. The dotted lines, showing the dependence of the vortex shedding frequency on Reynolds number in the inaudible range, intersect at origin.

l_0. Occasionally, however, especially at the higher Re, one may encounter higher vortex shedding frequencies such as $\frac{3}{2}f_0$, $2f_0$, etc., of which $\frac{3}{2}f_0$ is shown in Fig. 11.

A number of the more common jet-tone frequencies resulting from the process of vortex coalescence appear to be $\frac{2}{3}f_0$, $\frac{1}{2}f_0$, $\frac{1}{3}f_0$, $\frac{2}{5}f_0$, $\frac{1}{4}f_0$, $\frac{1}{5}f_0$, etc. when the vortex shedding frequency closest to the orifice is f_0. If the vortex shedding frequency also includes $\frac{3}{2}f_0$, then $\frac{3}{4}f_0$, etc. also appear. In Fig. 11 lines are drawn through the points $\frac{3}{2}f_0$, f_0, $\frac{2}{3}f_0$, $\frac{1}{2}f_0$, $\frac{2}{5}f_0$, $\frac{1}{3}f_0$, and $\frac{1}{4}f_0$ since these frequencies seemed to be observed the most often, with reasonable certainty, in the great number of shadowgraphs evaluated. Occasionally $\frac{3}{4}f_0$ and $\frac{1}{5}f_0$ were believed to be present. The plotting of these points together with the foregoing would account for some of the scattering of the points around $\frac{2}{3}f_0$ and $\frac{1}{4}f_0$ in Fig. 11. The audible jet-tone frequencies picked up by the microphone also fall on the solid lines.

Not all vortex separations observed in the shadowgraphs of a given jet over an extended period of time seem to lead to audible jet tones. To lead to audible tones, the vortex separations must occur often and regularly enough and the vortices must create a great enough disturbance. The range of Re at which the different jet-tone frequency components were audible are indicated, (Fig. 11) by the parts of the solid lines falling between two brackets.

The sequence arrangement of the vortex intervals appear to fluctuate very rapidly with time.

A shadowgraph at any one instant probably will not show vortex intervals corresponding to all the audible jet-tone frequencies picked up by a microphone. For example, in Figs. 6 and 7 of the frequencies 5350, 3563, 2673, 2140, 1782, and 1337 cps heard by the microphone, only vortex intervals corresponding to 5350(l_0), 3563($\frac{3}{2}l_0$), 2673($2l_0$), 1782($3l_0$), and 1337($4l_0$) were found. The vortex interval $\frac{5}{2}l_0$ corresponding to the jet-tone frequency 2140 picked up regularly by the microphone was not found in the shadowgraphs, however, but the two intervals $\frac{3}{2}l_0$ and l_0, whose sum equals the required vortex interval $\frac{5}{2}l_0$ were present. When this combination occurs with the two intervals $\frac{3}{2}l_0$ and l_0 adjacent, one might expect that the two intervals $\frac{3}{2}l_0$ and l_0 together will give rise in effect to a new derived interval $\frac{5}{2}l_0$. It appears then that these two intervals, if they occur often enough together, should give rise to the new frequency $\frac{2}{5}f_0$ (2140 cps) as well as the f_0 and $\frac{2}{3}f_0$. This may explain why no points, corresponding to the vortex separation $\frac{5}{2}l_0$, are associated with the solid line at $\frac{2}{5}f_0$ (Fig. 11).

On the other hand, even though the vortex pattern may contain a uniform sequence of vortex separations the microphone may not always pick up the corresponding jet-tone frequency. For example, in the studies at the Re of Figs. 9 and 10 and a number of others, the following frequencies, 6370, 5700, 4250, 3190, 2830, and 2175 cps were picked up by the microphone while vortex separations in the shadowgraphs corresponding

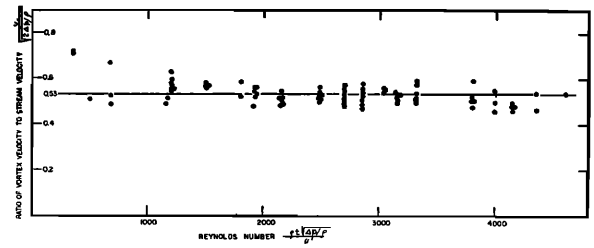

FIG. 12. Dependence of the ratio of vortex velocity to jet stream velocity on Reynolds number of jet.

to $\frac{2}{3}l_0$ (12 700 cps), l_0 (8500 cps), $\frac{4}{3}l_0$ (6370 cps), $\frac{3}{2}l_0$ (5700 cps), $2l_0$ (4250 cps), $\frac{8}{3}l_0$ (3190 cps), $3l_0$ (2830 cps), and $4l_0$ (2125 cps) were found. The frequencies 12 700 and 8500 cps should, however, have been picked up by the microphone according to the vortex separations observed in the shadowgraphs. They were probably not picked up because they were too weak in intensity in comparison with the jet noise at that frequency or did not occur frequently enough to make their presence readily detected. That is, their signal-to-noise ratio may have been too small.

The foregoing also is probably true for Fig. 8 at Re 1920 which is about the lowest Re at which jet tones were excited. Although the frequency 665 cps ($4l_0$) corresponds to none of the vortex intervals in Fig. 8, this interval actually did occur quite frequently in most of the other shadowgraphs made at this Re.

Figure 12 presents the dependence of the ratio $v/(2\Delta p/\rho)^{\frac{1}{2}}$ (of the vortex velocity v to the jet stream velocity expressed as $(2\Delta p/\rho)^{\frac{1}{2}}$, where Δp is pressure difference across the orifice and ρ is gas density) on Re of the jet (expressed as $\rho t(\Delta p/\rho)^{\frac{1}{2}}/\mu$), where t is orifice plate thickness and μ, viscosity of gas). This ratio was calculated from shadowgraphs of which Figs. 1 to 10 are typical.

No significant difference was found between the vortex velocity in the vicinity of the orifice before onset of coalescence and the vortex velocity downstream, especially after coalescence had run its course. Only in some intermediate positions, where a particular vortex was on the verge of coalescing with its neighbor did any significant differences appear. Accordingly, the average of the vortex velocities in a given jet appears to be quite representative of all the vortices in that jet and is the value of v in the velocity ratio of Fig. 12. The velocity ratio appears fairly independent of Re, within experimental scattering, even though jet-tone frequency and rate of shedding of vortices downstream from the orifice vary widely with change of Re. The result shown for jet tones in Fig. 12 agrees fairly well with that for pipe tones.[9]

DISCUSSION

Why jet tones generally are more feeble, unsteady, and uncertain than pipe tones[1,2] becomes apparent from a consideration of the shadowgraphs. Primary

pipe-tone shadowgraphs show the jet to be composed of an extremely uniform array of vortices fairly equal in size and spacing almost to the downstream point of dissolution of the jet vortex system. Jet-tone shadowgraphs, on the other hand, generally show a nonuniform array of vortices of different size and separation which, because of various forms of vortex coalescence, are different multiples of the separation of the vortices just emerging from the orifice.

Consideration of the shadowgraphs (Figs. 1 to 12) leads to the conclusion that the different regions of a jet should radiate different jet-tone frequencies. The higher frequencies should have their origin in the upstream region closest to the orifice, whereas, the lower frequencies should be radiated from the downstream region.

The shadowgraphs also indicate why the high-frequency jet tone f_0 is usually more clear and steady in amplitude than the lower jet-tone frequency components. The part of the vortex train in the shadowgraphs giving rise to f_0 flows directly out of the orifice, continuously and relatively uninterruptedly, while the parts of the vortex train giving rise to a particular low-frequency component are interspersed between vortex separations that give rise to other jet-tone frequencies. The vortex separations associated with a particular low-frequency jet tone occur, therefore, in bursts separated by other vortex separations.

Not all vortex trains appear to be acoustically active and to radiate perceptible sound. This does not appear due to lack in orderliness, periodicity, and continuity of the vortex train. For example, the vortex trains of Figs. 4 and 5 did not radiate a perceptible jet-tone frequency, yet they have more continuity and orderliness than many others obtained at higher Re that did radiate jet-tone frequencies. Lack of a perceptible jet tone here can not be due to small signal-to-noise ratio because the onset or disappearance of a jet tone with change of Re is always sudden, discontinuous, and quite perceptible. There may, however, be some hysteresis and variation from time to time in the value of the Re for onset or disappearance of a tone.

The vortices in the radiating vortex trains appear to be in a much more vigorous state of rotation, and the shadowgraphs of the vortices are more striated in appearance than in the nonradiating vortex trains according to the shadowgraphs.

The slope of the vortex shedding-frequency lines (Fig. 11) depends on whether the jet is radiating jet tones or not. When jet tones are audible, the points appear to fall on straight lines intersecting the axis at P around Re 1150. This trend agrees with results elsewhere.[1,3,4] The exact location of P would have been more obvious than appears from the figure if instead one had plotted the values of the audible jet-tone frequencies measured directly with a microphone. Since the points in Fig. 11 represent jet-tone frequencies calculated from vortex separations, they are subject to greater experimental error.

At the lower Re, on the other hand, where jet tones are not audible, the dependence of vortex shedding frequency on Re always appears to fall on the dotted lines intersecting the origin. In the transition region from inaudible to audible the points for a given Re may fall on either set of lines depending upon whether the jet happens to be radiating jet tones or not. The transition region occurs over a small Re interval. This accounts for the greater scattering of points in this region in Fig. 11.

Many of the vortex coalescences in the present studies appear to interact, qualitatively at least, as vortices might be expected to interact in a perfect fluid.[9] According to the latter, if a number of vortex rings coexist, each ring will move without sensible change of shape or size and with nearly uniform velocity in the direction of its rectilinear axis until it comes within short distance of a second ring. If the two circular vortices have the same rectilinear axis and the same sense of rotation, the two rings will advance in the same direction. Owing to their interaction, the ring-radius of the downstream vortex will increase causing its axial velocity of translation to decrease; the ring-radius of the upstream vortex will decrease causing its axial velocity of translation to increase. The upstream vortex ring should, therefore, overtake and pass through the downstream ring.

At this point, however, there exists a vital distinction between interaction of separate vortices in a perfect fluid and interaction of separate vortices in a viscous fluid. In the latter, the present studies show that a vortex may change in intensity by directly absorbing any number of others, the system coalescing into one or more distinct vortices, while at the same time their combined energies degrade gradually into heat. Never in the present studies, at least, was an upstream vortex found that penetrated and passed through a downstream vortex.

The process of vortex coalescence at low Re generally seems to approximate the foregoing most closely. Consider the interaction of vortices 2 and 3 (Fig. 3). The diameter of vortex 3 is increasing while its downstream translational velocity is decreasing. At the same time the diameter of vortex 2 is decreasing while its translational velocity is increasing leading finally to their coalescence as vortex 2, 3 on the right-hand shadowgraph.

The process of vortex coalescence at the higher Re appears to differ from the foregoing. Consider vortices 2 and 3 (Figs. 1 and 2). Upstream vortex 2 loses its identity long before it appears to have had time to move up smoothly into coincidence with downstream vortex 3. The identity and velocity of vortex 3, however, remains relatively little affected in the process of coalescence, although its intensity seems greater. That

is, vortex 3 affects the movement of vortex 2 before vortex 2 appears to have been able to affect the movement of the core of vortex 3.

This anomalous behavior at high Re might be accounted for by the consideration that the jet vortex train is farther from a steady state at high than at low Re. After vortex 3 (Figs. 1 and 2) has emerged from the orifice, it develops an induced velocity field[10] surrounding itself. When vortex 2 then emerges, it finds itself in this induced velocity field before vortex 2 has had time to develop its own sufficiently to affect the core of vortex 3. In the meantime, the induced velocity field of vortex 3 has caused vortex 2 to lose its identity while absorbing much of it.

At the lower Re, vortex 2 (Fig. 3) upon emergence, may still find itself in the induced velocity field of vortex 3. The field of vortex 3, however, may not be great enough materially to affect vortex 2 before vortex 2 has had time to develop its own. Therefore, there is soon a mutual interaction between the cores of the two vortices.

The normal vortex shedding frequency f_0 here is the same as the fundamental jet-tone frequency H_1 referred to elsewhere.[1]

[10] L. M. Milne-Thomson, *Theoretical Hydrodynamics* (The Macmillan Company, New York, 1950), pp. 313 and 493.

THE JOURNAL OF THE ACOUSTICAL SOCIETY OF AMERICA VOLUME 28, NUMBER 5 SEPTEMBER, 1956

Simple Form of the "Sing-Around" Method for the Determination of Sound Velocities*

GEORGE W. FICKEN, JR., AND E. A. HIEDEMANN
Department of Physics, Michigan State University, East Lansing, Michigan
(Received April 21, 1956)

An arrangement for the determination of sound velocities in liquids by means of measuring pulse repetition rates is described which, although very simple, allows an accuracy of better than 1%.

A SPECIAL form of the pulse method which R. L. Hanson[1] later aptly called a "sing-around" circuit was first described by H. Freund and E. Hiedemann[2] in a German patent application concerning a method to detect flaws in materials. The procedure consists in the use of a pulsed oscillator to drive a piezoelectric crystal which transduces the electrical into ultrasonic pulses in the medium with which the crystal is in contact. This pulse travels through the material to a second crystal acting as a receiver which reconverts the ultrasonic into an electrical pulse. The pulse is amplified, detected, and instantaneously fed back to the oscillator to trigger the next outgoing pulse. The frequency of the pulse sequence depends on the path length and the ultrasonic velocity in the medium. Measuring the pulse repetition rate allows, therefore, the measurement of the sound velocity. The presence of flaws in materials is indicated by incorrect values of the measured "apparent" sound velocity. Although a brief description of the method was given later at a somewhat more accessible place,[3] it attracted not much attention until it was used and developed by R. D. Holbrook,[4] Cedrone and Curran,[5] and H. Schmauch.[6] The latest development by M. Greenspan and E. Tschiegg[7] has proved that the method can be used for very precise measurements of sound velocities. Furthermore, the principle of the method is used in a commercial thickness meter[8] in the form of analyzing multiple echoes.

In view of the renewed interest in the sing-around circuit, we felt that a brief report on a very simple form of the setup might be of interest.

Figure 1 shows a block diagram of the entire apparatus. A positive pulse from the multivibrator generates an ultrasonic pulse at the transmitting transducer which travels through the material until it impinges on the receiving transducer, where it produces an electrical pulse which, in turn, is used to trigger the multivibrator. If the delay time in the electronic circuit

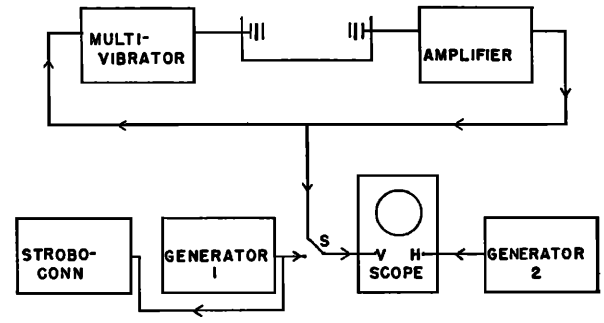

FIG. 1. Block diagram.

* Sponsored by the Office of Ordnance Research, U. S. Army.
[1] R. L. Hanson, J. Acoust. Soc. Am. 21, 60 (1949).
[2] H. Freund and E. Hiedemann, German Patent Appl. (1940).
[3] E. Hiedemann, FIAT Rev. Ger. Sci. 1939–1946, Part I, 178 (1947).
[4] R. D. Holbrook, J. Acoust. Soc. Am. 20, 590 (1948).
[5] N. P. Cedrone and D. R. Curran, J. Acoust. Soc. Am. 26, 963 (1954).
[6] H. Schmauch, Ann. Univ. Savaviensis 2, (3), 257–269 (1953).
[7] M. Greenspan and C. E. Tschiegg, J. Acoust. Soc. Am. 28, 158 (1956).
[8] J. Krautkrämer, Z. Metallkunde 45, 154 (1954).